ACS APPLIED MATERIALS & INTERFACES

Research Article

www.acsami.org

Investigating Local Degradation and Thermal Stability of Charged Nickel-Based Cathode Materials through Real-Time Electron Microscopy

Sooyeon Hwang,[†,‡,∥] Seung Min Kim,[⊥] Seong-Min Bak,[†,◇] Byung-Won Cho,[†] Kyung Yoon Chung,[†] Jeong Yong Lee,*[,‡,§] Wonyoung Chang,*[,†] and Eric A. Stach*[,∥]

[†]Center for Energy Convergence, Korea Institute of Science and Technology, Seoul 136-791, Republic of Korea

[‡]Department of Materials Science and Engineering, KAIST, Daejeon 305-701, Republic of Korea

[§]Center for Nanomaterials and Chemical Reactions, Institute for Basic Science, Daejeon 305-701, Republic of Korea

[∥]Center for Functional Nanomaterials, Brookhaven National Laboratory, Upton, New York 11973, United States

[⊥]Carbon Convergence Materials Research Center, Korea Institute of Science and Technology, Wanju-gun 565-905, Republic of Korea

Supporting Information

ABSTRACT: In this work, we take advantage of in situ transmission electron microscopy (TEM) to investigate thermally induced decomposition of the surface of $Li_xNi_{0.8}Co_{0.15}Al_{0.05}O_2$ (NCA) cathode materials that have been subjected to different states of charge (SOC). While uncharged NCA is stable up to 400 °C, significant changes occur in charged NCA with increasing temperature. These include the development of surface porosity and changes in the oxygen K-edge electron energy loss spectra, with pre-edge peaks shifting to higher energy losses. These changes are closely related to O_2 gas released from the structure, as well as to phase changes of NCA from the layered structure to the disordered spinel structure, and finally to the rock-salt structure. Although the temperatures where these changes initiate depend strongly on the state of charge, there also exist significant variations among particles with the same state of charge. Notably, when NCA is charged to $x = 0.33$ (the charge state that is the practical upper limit voltage in most applications), the surfaces of some particles undergo morphological and oxygen K-edge changes even at temperatures below 100 °C, a temperature that electronic devices containing lithium ion batteries (LIB) can possibly see during normal operation. Those particles that experience these changes are likely to be extremely unstable and may trigger thermal runaway at much lower temperatures than would be usually expected. These results demonstrate that in situ heating experiments are a unique tool not only to study the general thermal behavior of cathode materials but also to explore particle-to-particle variations, which are sometimes of critical importance in understanding the performance of the overall system.

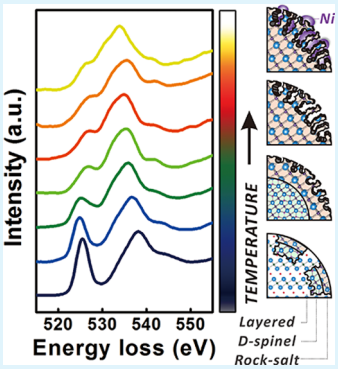

KEYWORDS: *lithium ion batteries, Ni-based cathode, thermal degradation, in situ transmission electron microscopy, electron energy loss spectroscopy*

INTRODUCTION

Today's wireless technology provides ubiquitous web access through mobile devices such as smartphones, tablets, and laptops with the help of lightweight and powerful energy sources in the form of lithium ion batteries (LIB). LIB technology is preparing for the next step, namely, larger-scale applications such as incorporation into electric vehicles[1] and "smart grids".[2] Because of their high energy density, nickel-based layered positive electrode materials are being considered as one of the prime candidates for alternative cathode materials, particularly for automobile applications. The most frequently used commercial cathode material in LIBs is $LiCoO_2$, yet only half of its theoretical capacity can be used.[3] By comparison, $LiNiO_2$ can provide 65% of its theoretical capacity,[4] and thus Ni-rich cathode materials deliver 30% more energy than $LiCoO_2$.[5] Additionally, Ni is more cost-effective and less toxic than Co.[6]

Despite these advantages, the thermal instability of Ni-rich materials is the largest hurdle that must be overcome before their widespread usage. The Ni^{4+} ions in charged Ni-rich materials are thermodynamically unstable and have a strong driving force to reduce to Ni^{2+}, leading to phase transformations from an original layered structure (space group $R\bar{3}m$) to a disordered spinel structure ($Fd\bar{3}m$), and finally to a rock-salt structure ($Fm\bar{3}m$) with increasing temperature.[7] Further reduction of Ni ions with increasing temperature eventually results in the nucleation of Ni metal particles.[8] These

Received: May 26, 2014
Accepted: August 6, 2014
Published: August 7, 2014

phase transitions are extremely detrimental to the safety of LIB because the phase transitions are accompanied by the release of oxygen gas from the cathode materials, provoking a catastrophic explosion through further reactions with the flammable electrolyte.[9] Electric vehicles are powered by much larger LIBs than those used to power mobile devices and are always exposed to the possibility of a sudden crash. Crashes can engender a huge amount of heat, potentially leading to explosive failure of on-board batteries. Thus, a systematic and reliable diagnosis of the thermal stability of Ni-rich cathode materials is a prerequisite for the incorporation of these materials into electric vehicle applications.

Extensive studies have been conducted to investigate the thermal behavior of Ni-rich cathode materials, including the use of thermogravimetric analysis (TGA), differential scanning calorimetry (DSC)[10] coupled with mass spectroscopy (MS),[11] accelerating rate calorimetry (ARC),[12] normal or time-resolved X-ray diffraction (TR-XRD),[7,13,14] and X-ray absorption spectroscopy (XAS).[7] These studies have provided significant insights into the average, bulk behavior of Ni-rich cathode materials. However, in order to fully understand the performance of a system, it is sometimes more important to investigate the evolution of surfaces rather than the bulk, as well as to consider variations among particles rather than average properties. The surface regions of electrode materials—which are the locations of the electrochemical reaction fronts between the cathode and the electrolyte—experience significantly more harsh conditions than the bulk due to the presence of an overpotential caused by relatively slow Li diffusion into the electrode. Our recent work demonstrated that inhomogeneity in both the crystallographic and electronic structures of $Li_xNi_{0.8}Co_{0.15}Al_{0.05}O_2$ (NCA) cathode materials can develop at the near-surface region following the initial charge at room temperature, even though the bulk still maintains its original crystal structure. We also found that there exist significant variations in the degree of surface inhomogeneity among particles, even with the same state of charge (SOC).[15] Therefore, in order to understand how thermal excursions to higher temperatures affect the performance and safety of these materials, it is imperative to investigate the local evolution of surface structure, as well as variations in the evolution of individual particles during heat treatment. Transmission electron microscopy (TEM) is uniquely able to probe the nanoscale evolution of surface morphology, crystal structure, and electronic structure in materials. In addition, the ability to subject samples to thermal excursions in situ to the TEM allows direct investigation of the effect of heat on the evolution of materials morphology.[16]

Here, we use in situ bright-field (BF) imaging, high-resolution electron microscopic (HREM) imaging, selected-area electron diffraction (SAED), and electron energy loss spectroscopy (EELS) to monitor the morphological, structural, and chemical evolution of the surface of NCA particles with increasing temperature as a function of charging depth. Previous studies using X-ray spectroscopic techniques have established that the state of charge highly affects the temperature at which the structural evolution of NCA particles initiates.[7] However, a global average technique such as XAS or XRD cannot reveal either the specific location or the mechanism by which thermal decomposition initiates and propagates into the particle bulk. In prior work, Wu et al.[14] utilized in situ TEM to characterize the phase transitions that occur in overcharged $Li_xNi_{0.8}Co_{0.15}Al_{0.05}O_2$ ($x < 0.15$). They showed that phase transitions occur even at room temperature and that they can proceed toward the inner region of the particles with increases in temperature.[14] However, this study did not systematically investigate the effect of different SOC on morphological evolution. In addition, there has been no systematic study of the variation in onset temperatures for these morphological changes among different particles, at the same state of charge. Here, we have analyzed the thermal decomposition of seven different NCA particles with the charge state of $x = 0.33$, the charge state that is the practical upper limit voltage when charging LIB in most applications. Surprisingly, we have observed huge variations among particles with the same state of charge, which is a significant observation that has important ramifications on LIB performance. This study demonstrates the utility of real-time transmission electron microscopy to understand the detailed thermal behavior of cathode materials for next-generation LIBs.

EXPERIMENTAL DETAILS

Nickel-rich cathode materials—$Li_xNi_{0.8}Co_{0.15}Al_{0.05}O_2$, referred to as NCA (a commercial product)—were electrochemically delithiated at a rate of $C/10$ under galvanostatic conditions until they had remaining lithium compositions of $x = 0.5$, 0.33, and 0.1. The cathode part was prepared from a mixed slurry of 90 wt % active material (NCA), 6 wt % conducting carbon, and 4 wt % poly(vinylidene difluoride) (PVDF) binder in *N*-methylpyrrolidone (NMP) solvent. This slurry was then coated onto an Al foil, which acted as a current collector. The cathode was incorporated with Li metal as an anode, a Celgard separator, and an electrolyte of 1 M $LiPF_6$ dissolved in ethylene carbonate (EC), ethyl methyl carbonate (EMC), and dimethyl carbonate (DMC) solvent (1:1:1 by volume) to assemble a 2032-type coin cell. The galvanostatic charging profile is shown in Supporting Information (Figure S1).

After reaching the state of $x = 0.5$ ($Li_{0.5}$NCA), $x = 0.33$ ($Li_{0.33}$NCA), or $x = 0.1$ ($Li_{0.1}$NCA), the coin cells were disassembled, and the cathode was immersed in a pure DMC solution to clean off the residual salts. The remaining lithium content was estimated by the charge passed through the cell and the mass of active material, based on the theoretical capacity of 280 mA·h/g, with the assumption of 100% coulombic efficiency. Charged particles were acquired for subsequent analysis by gentle abrasion of the Al foil. Supersonic vibration was applied to ensure good dispersion of powder samples in a small vial with pure DMC solution before they were dropped onto a lacey carbon TEM grid. Sample preparation and loading into a TEM sample holder were done in either an argon-filled glovebox or in a dry room, and the TEM sample holder was then transferred to the microscope in a hermetically sealed container to minimize exposure of the samples to air and moisture. Total exposure to air was on the order of 10 s.

Changes occurring in the surface of charged NCA cathode material during heating were observed in real time with JEM-2100F (JEOL) and Tecnai G^2 F20 (FEI) TEMs at an accelerating voltage of 200 kV, and a spherical aberration-corrected environmental TEM (FEI Titan 80/300 ETEM with CEOS C_s corrector) at an accelerating voltage of 300 kV. The thermal behavior of NCA was investigated while increasing the temperature from room temperature (25 °C) to 400 °C by use of a 652 double-tilt heating holder (Gatan) or an Aduro heating holder (Protochips). Electron energy loss (EEL) spectra were acquired on a GIF Tridiem system (Gatan). Energy resolution of the EEL spectrum—determined by measuring the full width at half-maximum of the zero loss peak (ZLP)—was around 1 eV. The backgrounds of all spectra were subtracted via the power law method embedded in Digital Micrograph software (Gatan).

RESULTS AND DISCCUSION

Pristine NCA (before charging) was first investigated as a reference. The morphology of pristine NCA shows no

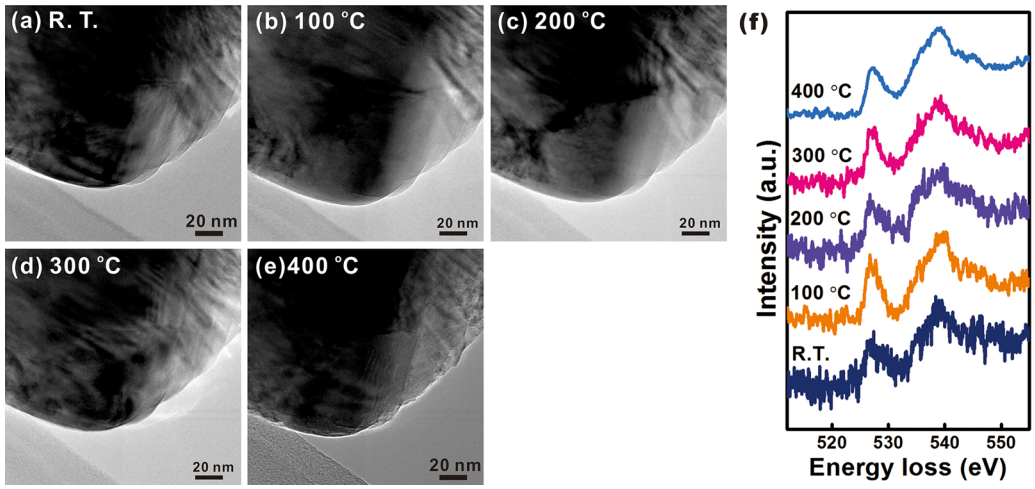

Figure 1. (a–e) Real-time BF images of the surface of pristine NCA (before charging) from room temperature to 400 °C. (f) Oxygen K-edge EEL spectra acquired from the area indicated in panels a–e.

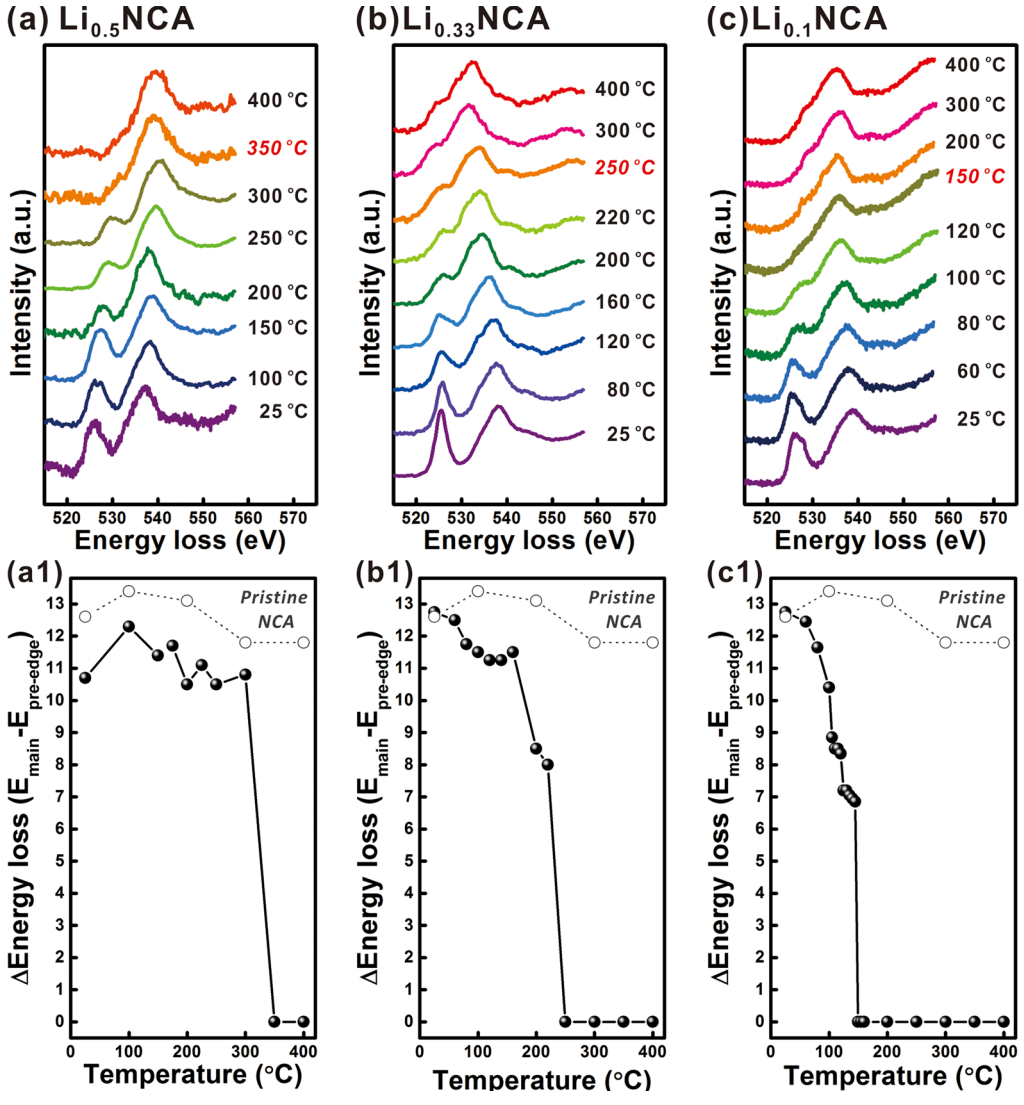

Figure 2. (Top row) Temperature dependence of oxygen K-edge EEL spectra from (a) $Li_{0.5}NCA$, (b) $Li_{0.33}NCA$, and (c) $Li_{0.1}NCA$. (Bottom row) Changes in ΔE values with increasing temperature from (a1) $Li_{0.5}NCA$, (b1) $Li_{0.33}NCA$, and (c1) $Li_{0.1}NCA$. ΔE values from a pristine sample are shown for comparison.

dx.doi.org/10.1021/am503278f | ACS Appl. Mater. Interfaces 2014, 6, 15140–15147

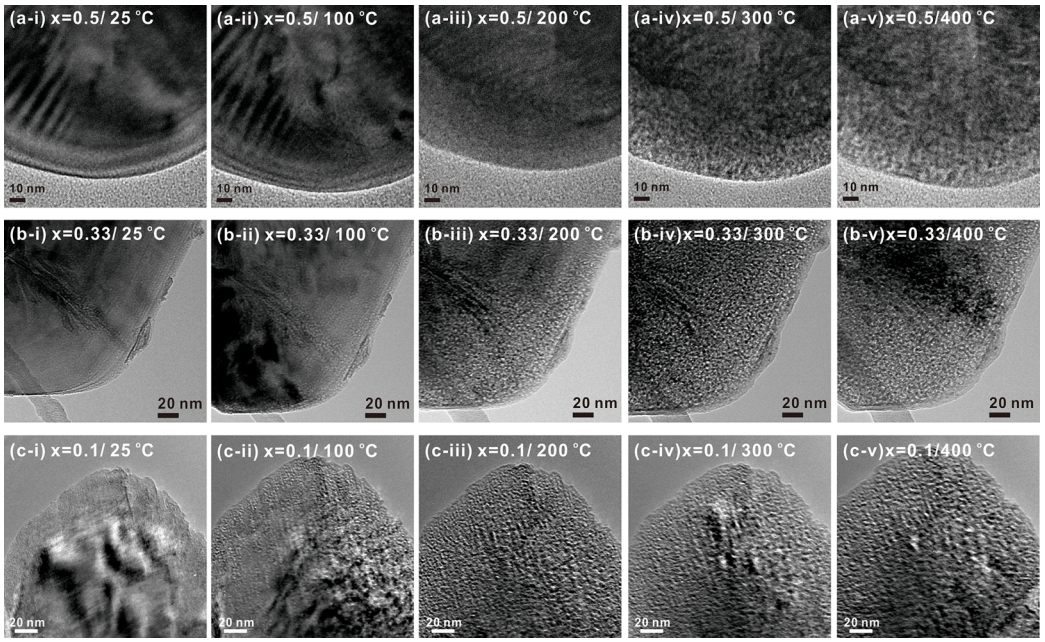

Figure 3. Real-time BF images of the surface of (row a) $Li_{0.5}NCA$, (row b) $Li_{0.33}NCA$, and (row c) $Li_{0.1}NCA$ during heating.

significant change from room temperature to 400 °C (Figure 1a−e). EEL spectra, which measure the density of states above the Fermi level,[17] are used to investigate changes in the electronic structure of NCA upon heating. Oxygen attracts special attention because oxygen gas is liberated from charged NCA upon heating, accompanying the sequential phase transformations of charged NCA.[7] Additionally, the liberated oxygen gas reacts with flammable electrolytes in the battery structure, generating additional heat. Furthermore, the near-edge structure of the oxygen K-edge provides direct insight into the oxidation state of the transition metals in these materials,[18] and thus oxygen is a key element to assess when safety issues during thermal decomposition are considered. Oxygen K-edge EEL spectra were acquired from the same area of Figure 1a−e. All spectra show two distinct peaks. The first peak, referred as a pre-edge peak (at ≈528 eV), is attributed to a transition of electrons from the O 1s state to unoccupied O 2p states that are hybridized with the 3d state of transition metals (TM), which is dominantly the Ni in NCA. The second peak, referred to as the main peak (at around 540 eV), is attributed to a transition of electrons from O 1s core state to empty O 2p−Ni 4sp hybridized states.[19] All spectra were normalized to the intensity of the main peak. Each spectrum taken from room temperature to 400 °C shows a similar fingerprint (Figure 1f), indicating that both the electronic structure and the morphology near the surface of pristine NCA are thermally stable up to 400 °C.

Figure 2 presents oxygen K-edge EEL spectra of charged $Li_xNi_{0.8}Co_{0.15}Al_{0.05}O_2$ as a function of charging depth [x = 0.5 ($Li_{0.5}NCA$), x = 0.33 ($Li_{0.33}NCA$), and x = 0.1 ($Li_{0.1}NCA$)] obtained during in situ heating. To follow the changes in the electronic structure, EEL spectra were acquired at the same area at each temperature. As the temperature increases, the pre-edge peak shifts toward a higher energy loss, eventually becoming more or less a shoulder of the main peak. This indicates that considerable changes occur in the electronic structure of the charged material, even though the oxygen K-edges of pristine NCA maintain the initial feature of two distinctive peaks, even to temperatures as high as 400 °C. The temperature at which the pre-edge peak is no longer discernible becomes lower with increasing depth of charge: 350, 250, and 150 °C for $Li_{0.5}NCA$, $Li_{0.33}NCA$, and $Li_{0.1}NCA$, respectively (Figure 2a−c). The change in energy loss between the main and pre-edge peaks (ΔE) as a function of temperature is shown in Figure 2a1−c1 for clarity. ΔE values for pristine NCA extracted from Figure 1f are superimposed for comparison. With increasing charge depth, ΔE changes more quickly upon heating, implying a faster modification of the electronic structure with deeper charge. XAS, which has superior energy resolution when compared with conventional EELS, has shown that the valence states of the TM affect the pre-edge peak of the oxygen K-edge. Specifically, the transitions of electrons from O 1s to O 2p−$Ni^{3+/4+}$ 3d hybridized states and to O 2p−Ni^{2+} 3d hybridized states form pre-edge peaks at 528.5 and 531.8 eV, respectively.[20] Therefore, the positive shift of the pre-edge peak and the smaller ΔE values indicate that the Ni ions in the NCA material are being reduced.

Figure 3 presents changes in morphology that occur at the surface at each state of charge. Upon heating, nascent porosity arises at the edge of the particles and propagates toward the bulk. With increasing depth of charge, the changes in morphology initiate at lower temperatures. Noticeable porosity is seen at 300, 200, and 100 °C for $Li_{0.5}NCA$, $Li_{0.33}NCA$, and $Li_{0.1}NCA$, respectively. Ni ions in Ni-rich cathode materials are oxidized to Ni^{4+} during charging: these Ni^{4+} ions are known to be unstable and tend to further reduce to more stable valence states, which is accompanied by both phase transitions and gas evolution at elevated temperatures.[21] This gas evolution is correlated with the formation and propagation of porosity seen in these images. Previous time-resolved X-ray diffraction (TR-XRD) studies have been correlated with mass spectroscopy (MS) measurements and have shown that oxygen gas is released from half-charged NCA ($Li_{0.5}NCA$) at 200−275 °C.[7] Solely from consideration of the stoichiometry of NCA, there is no reason for oxygen gas to be released upon the initial phase transition from layered structure to disordered spinel for half-

charged NCA ($Li_{0.5}$NCA). Bak et al.[7] inferred that the surfaces of half-charged NCA should be more charged than the bulk, leading to oxygen release from the surface area. Our real-time TEM experiments clearly demonstrate that incipient porosity at the surface appears for $Li_{0.5}$NCA around 200 °C (Figure 3 , panel a-iii) and porosity becomes prevalent at 300 °C (Figure 3 , panel a-iv): these observations of porosity are well matched to the unexpected oxygen evolution detected by TR-XRD coupled with MS.[7] In our recent work, we found that incipient phase transitions occur at the edge of the $Li_{0.5}$NCA particles even at room temperature after an initial charge.[15] In situ BF images shown in Figure 3, row a, provide clear evidence that thermal decomposition can initiate at lower temperatures in the near surface region than in the bulk, leading to the sudden release of oxygen gas from the cathode materials. Along with changes in the morphology and electronic structure, a modification in the crystallographic structure of Li_xNCA occurs concurrently with the increase in temperature: specifically a change from the layered $R\bar{3}m$ to the disordered spinel ($Fd\bar{3}m$) and finally to the rock-salt ($Fm\bar{3}m$) structure, as shown in the Supporting Information, Figures S2 (x = 0.5) and S3 (x = 0.1). As the amount of lithium extracted from the structure increases, we find that the phase transitions occur at lower temperature.

It should be noted that the temperatures at which the porosity becomes significant are well-matched with the temperatures at which oxygen pre-edge peaks of $Li_{0.5}$NCA, $Li_{0.33}$NCA, and $Li_{0.1}$NCA particles disappear in Figure 2a–c. The development of surface porosity is a visible phenomenon that is most likely caused by oxygen gas release. Oxygen gas is liberated from the charged NCA during heat treatment in order to maintain charge neutrality when highly unstable Ni^{4+} ions reduce to Ni^{2+} ions.[7] The Ni reduction accompanies the sequential phase transitions from the layered to the disordered spinel and finally to the rock-salt structures at high temperature and causes the pre-edge peak of the oxygen K-edge to move toward the main peak. All these phenomena are intimately related.

When the safety of LIBs is considered, it is important to consider the material condition at the highest operating voltage, as that corresponds to the highest energy state. Practical utilization of LIBs occurs at voltages ranging from 3.0 to 4.2 V, and at 4.2 V nearly 67% of lithium is extracted from pristine NCA (Supporting Information Figure S1). Thus, we focus particular attention on $Li_{0.33}$NCA particles. Figure 4 presents further examples of $Li_{0.33}$NCA particles, specifically those that showed even severer evolution of their surface morphology than the $Li_{0.33}$NCA particle shown in Figure 3, row b. In the examples shown in Figure 4 , panels a-iii and b-iii, nanoparticles are nucleated on the edges of $Li_{0.33}$NCA particles at 400 °C. Selected-area electron diffraction (SAED) patterns from the surface area of NCA (Figure 4, panel b-vi) show extra spots, indicating that there exists a new crystalline phase along with the pre-existing rock-salt structure of NCA. Based on the lattice parameters (a = 4.13 Å for $LiNiO_2$ of rock-salt structure[22] and a = 3.52 Å for Ni), the extra spots are consistent with the presence of metallic Ni. Yoon et al.[8] have previously used TR-XRD to show that metallic Ni is produced when $Li_{0.33}NiO_2$ is heated in the presence of an electrolyte.

Figure 5a shows a HREM image acquired at the surface of $Li_{0.33}$NCA at 400 °C, which undergoes an even severer morphological change. A fast Fourier transformation (FFT) of the entire HREM image (Figure 5a) in Figure 5c indicates that the bulk of the particle is oriented along the 110 zone-axis

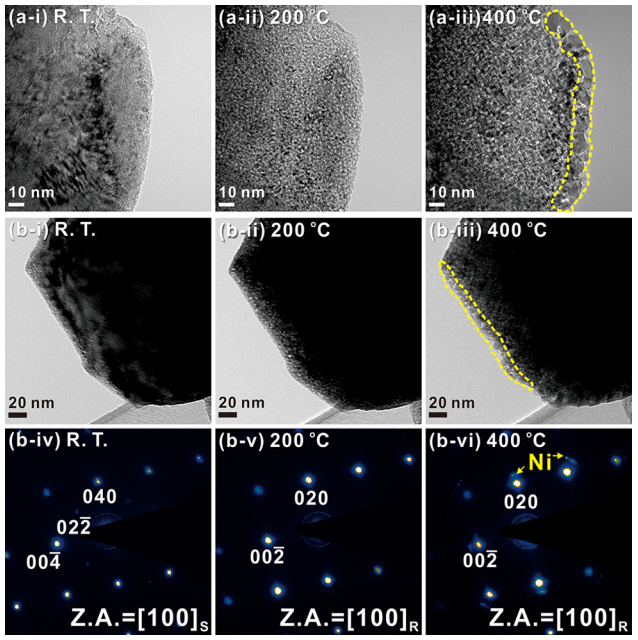

Figure 4. (Rows a and b, panels i–iii) BF images representing generation of Ni nanoparticles at the surface of $Li_{0.33}$NCA with increasing temperature. (Row b, panels iv–vi) Selected-area diffraction patterns acquired from row b, panels i–iii, respectively. S and R denote the spinel and rock-salt structures, respectively.

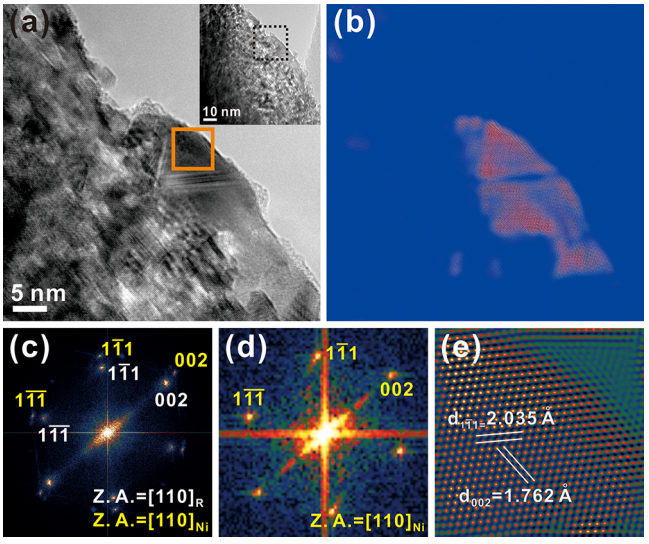

Figure 5. (a) HREM image acquired from the edge of a $Li_{0.33}$NCA particle. (Inset) Area of the particle from which the HREM image is taken. (b) Inverse FFT image produced only with the contribution of the metallic Ni phase. (c) FFT result from whole HREM image in panel a. R indicates the rock-salt structure. (d) FFT result from the orange boxed area in panel a. (e) Inverse FFT result of panel d.

of the rock-salt structure of NCA, but there also exists metallic Ni, with the two phases having similar crystallographic orientation and symmetry. The initial stage of reduction from NiO to Ni is known as a topotactic reaction, meaning that each plane of Ni is parallel to the corresponding plane in NiO.[23] In order to spatially locate the distribution of the metallic Ni, Figure 5b presents the commensurate inverse FFT image of Figure 5a produced by selecting spots from only the Ni metal in Figure 5c. Most of the pure Ni particles exist at the edge of the

NCA mother particle, consistent with the observation that the surface area undergoes the severest decomposition. Figure 5d is a FFT taken from the orange box in Figure 5a, and Figure 5e is an inverse FFT image obtained by selecting the spots of the FFT in Figure 5d. The measured lattice spacings in Figure 5e correspond to those of the Ni 111 and 200 planes, again confirming the nucleation of metallic Ni nanoparticles on the edges of mother NCA particles. These results clearly show that there are distinct variations in the extent of morphological evolution among the $Li_{0.33}$NCA particles, even at the same state of charge.

As mentioned earlier, the position of the oxygen K-edge pre-edge peak and ΔE depend strongly on the oxidation state of Ni, and thus demonstrate that Ni is being reduced with increasing temperature for charged NCA particles. When it is considered that NiO with the rock-salt structure still has a distinctive pre-edge peak of oxygen K-edge EEL spectra,[24] the disappearance of the pre-edge peak in Figure 2 indicates a weakening of the hybridization between Ni 3d and O 2p states and is expected to correlate with further reduction of Ni^{2+} ions to metallic Ni, as presented in Figures 4 and 5. Analysis of the Ni $L_{2,3}$ edges also indicates Ni reduction. However, we find that the changes in the oxygen K-edge are more conspicuous than those that occur in the Ni $L_{2,3}$ edges with increasing temperature, and thus we have focused our attention on the oxygen K-edge within the main text. Additional information regarding the Ni $L_{2,3}$ edges can be found in the Supporting Information, specifically Figure S4.

In addition to the structural changes described above, there are also strong particle-to-particle variations in the near-surface electronic structure in $Li_{0.33}$NCA, as indicated by the difference in temperature dependence of the observed modification of oxygen K-edges. Figure 6 presents two extremes, of early (a)

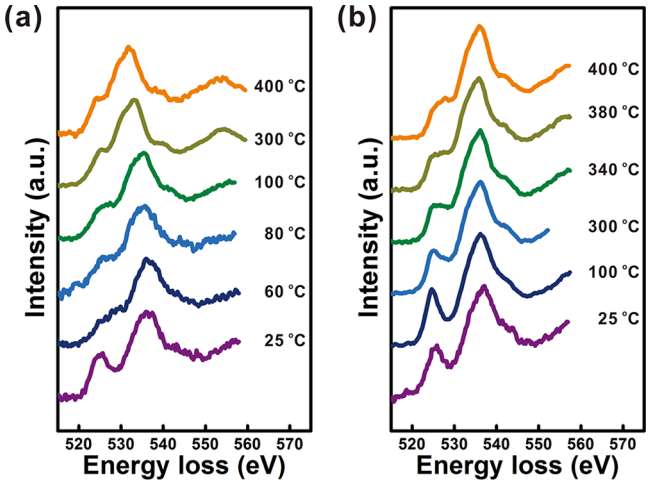

Figure 6. Representative oxygen K-edge EEL spectra of $Li_{0.33}$NCA representing (a) early and (b) late transitions of the pre-edge peak with increasing temperature.

and late (b) transitions of the oxygen K-edge pre-edge peaks of $Li_{0.33}$NCA with increasing temperature. In the case of the early transition, the oxygen pre-edge peak becomes significantly reduced in intensity upon reaching only 60 °C (Figure 6a), while the oxygen pre-edge peak is clearly distinguishable well above 300 °C for the other particle (Figure 6b). Real-time bright-field images of $Li_{0.33}$NCA particles with early and late ΔE transitions are provided in the Supporting Information, Figure S5.

The inhomogeneity in the response of individual particles is further examined in Figure 7 by plotting the variation in ΔE

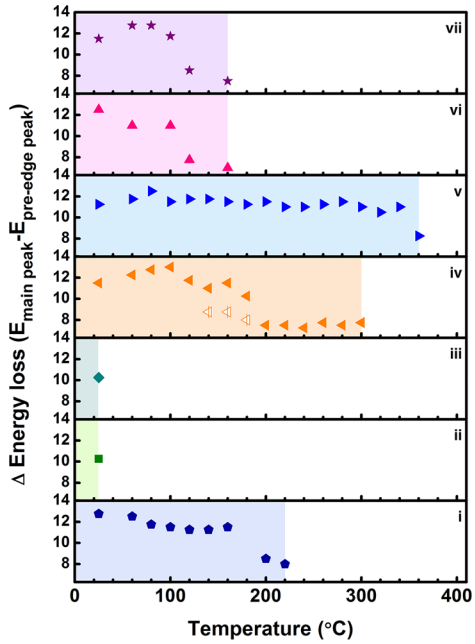

Figure 7. Variation in electronic structure of $Li_{0.33}$NCA, as indicated by changes in ΔE values with increasing temperature.

versus temperature for seven different particles. We have chosen to plot ΔE because it reflects the movement of the pre-edge peak and thus the reduction of Ni ions, as described above. Most particles (Figure 7 , panels i, iv, v, vi, and vii) exhibit a stepwise decrease in ΔE prior to a distinct transition temperature at which the pre-edge peak becomes essentially overlapped with the main peak (i.e., $\Delta E \rightarrow 0$), indicating a progressive reduction of Ni ions. In the case of Figure 7 , panel iv, the pre-edge is split into two peaks: this implies that the positive electrode has more than one valence state as the Ni reduction occurs (from 140 to 180 °C). Figure 7 panels ii and iii demonstrate that $Li_{0.33}$NCA particles can be thermally unstable even at 60 °C, as indicated by the early disappearance of the pre-edge peak.

The observed differences in thermal decomposition behavior can be caused by a number of factors, including kinetic effects that occur during initial charge or heating, inhomogeneous dispersion of active materials, conducting agents, and polymer binder in the mixed slurry of the cathode, and the degree of electrolyte impregnation into the cathode. The prime concern here is the fact that even within the normal voltage range of LIBs, substantial particle-by-particle variations are observed upon thermal decomposition. Even more critically, a small portion of particles can be decomposed and potentially instigate thermal runaway inside a battery at temperatures as low as 60 °C, which is low enough to be a threat during normal operation.

Figure 8 summarizes schematically the changes observed in $Li_{0.33}$NCA cathode materials over the temperature range from room temperature to 400 °C. As the temperature increases, major changes occur in the morphology as well as the crystallographic and electronic structures of the charged

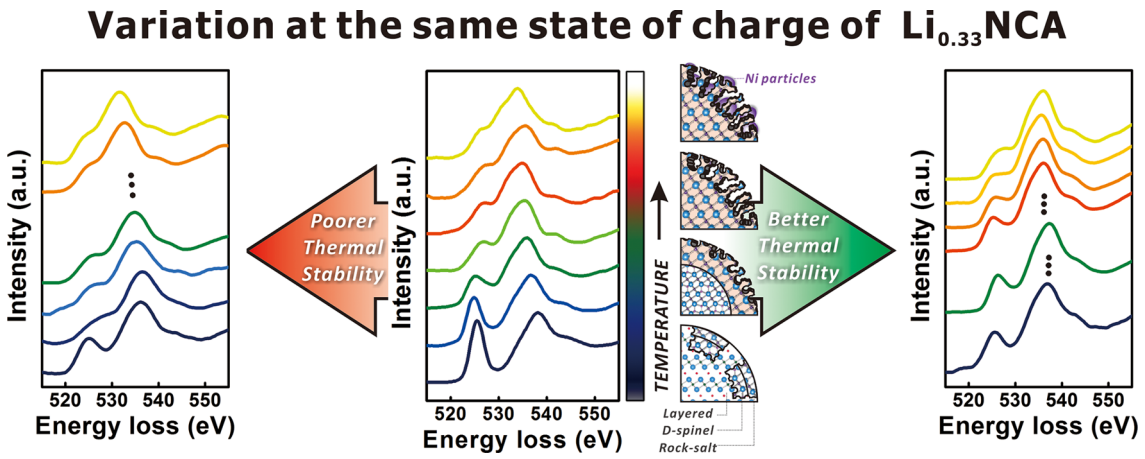

Figure 8. Scheme that summarizes thermal decomposition of charged NCA in terms of electronic structure and morphology.

particles. These modifications are closely correlated, resulting from reduction of the transition metal and the associated gas evolution with increasing temperature. The degree of thermal decomposition is not homogeneous from particle to particle, even at the same state of charge and temperature, and significant variation is observed in the temperature dependence of the oxygen K-edge EEL spectra.

CONCLUSION

Real-time TEM has been used to describe the thermal decomposition that occurs at the surface of $Li_xNi_{0.8}Co_{0.15}Al_{0.05}O_2$ cathodes. We have observed that with increasing temperatures there is a development of surface porosity, which is directly correlated with shifts of the oxygen K-edge pre-edge peak to higher energy loss. This observation is closely related to the reduction of unstable Ni^{4+} ions, oxygen gas release, and sequential phase transformations. These changes are interrelated and not only depend on the state of charge but also exhibit particle-to-particle variations. For $Li_{0.33}NCA$, which is in the highest energy state in practical usage, there are huge variations in the onset temperature among the particles. Some particles undergo considerable thermal decomposition even below 100 °C. This temperature can be reached during a normal operation of devices that are powered by LIB, and thus these particles can initiate thermal runaway at lower temperatures than usually expected. This study shows that in order to guarantee the safe operation of LIB, it is necessary not only to understand the bulk thermal behavior but also to explore particle-to-particle variations by nanoscale characterization techniques.

ASSOCIATED CONTENT

Supporting Information

Additional text and five figures, showing voltage profiles of $Li_{0.5}NCA$, $Li_{0.33}NCA$, and $Li_{0.1}NCA$ during electrochemical delithiation; analysis of SAED patterns of $Li_{0.5}NCA$ and $Li_{0.1}NCA$ and Ni $L_{2,3}$ edges of $Li_{0.33}NCA$ samples with increasing temperature; and corresponding bright-field images of the surface area of $Li_{0.33}NCA$ particles showing early and late transition in ΔE of oxygen K-edge in Figure 6. This material is available free of charge via the Internet at http://pubs.acs.org.

AUTHOR INFORMATION

Corresponding Authors

*E-mail j.y.lee@kaist.ac.kr.
*E-mail cwy@kist.re.kr.
*E-mail estach@bnl.gov.

Present Address

◊Chemistry Department, Brookhaven National Laboratory, Upton, New York 11973, United States.

Author Contributions

The manuscript was written through contributions of all authors. All authors have given approval to the final version of the manuscript.

Notes

The authors declare no competing financial interest.

ACKNOWLEDGMENTS

This work was supported by the Korea Institute of Science and Technology (KIST) Institutional Program (Projects 2E25086 and 2Z04020). This work was also supported by the National Research Foundation of Korea, funded by the Korean Government (MEST) (Grant NRF-2011-C1AAA001-0030538). Research was partially carried out at the Center for Functional Nanomaterials, Brookhaven National Laboratory, which is supported by the U.S. Department of Energy, Office of Basic Energy Sciences, under Contract DE-AC02-98CH10886.

REFERENCES

(1) Armand, M.; Tarascon, J.-M. Building Better Batteries. *Nature* **2008**, *451*, 652−657.
(2) Dunn, B.; Kamath, H.; Tarascon, J.-M. Electrical Energy Storage for the Grid: A Battery of Choices. *Science* **2011**, *334*, 928−935.
(3) Whittingham, M. S. Lithium Batteries and Cathode Materials. *Chem. Rev.* **2004**, *104*, 4271−4301.
(4) Chebiam, R. V.; Kannan, A. M.; Prado, F.; Manthiram, A. Comparison of the Chemical Stability of the High Energy Density Cathodes of Lithium-Ion Batteries. *Electrochem. Commun.* **2001**, *3*, 624−627.
(5) Manthiram, A. In *Lithium Batteries: Science and Technology*; Nazri, G.-A., Pistoia, G., Eds.; Springer: New York, 2003; Chapt. 1, pp 3−41.
(6) Zhang, Y.; Wang, C.-Y. Cycle-Life Characterization of Automotive Lithium-Ion Batteries with $LiNiO_2$ Cathode. *J. Electrochem. Soc.* **2009**, *156*, A527−A535.
(7) Bak, S.-M.; Nam, K.-W.; Chang, W.; Yu, X.; Hu, E.; Hwang, S.; Stach, E. A.; Kim, K.-B.; Chung, K. Y.; Yang, X.-Q. Correlating Structural Changes and Gas Evolution during the Thermal Decomposition of Charged $Li_xNi_{0.8}Co_{0.15}Al_{0.05}O_2$ Cathode Materials. *Chem. Mater.* **2013**, *25*, 337−351.

(8) Yoon, W.-S.; Chung, K. Y.; Balasubramanian, M.; Hanson, J.; McBreen, J.; Yang, X.-Q. Time-Resolved XRD Study on the Thermal Decomposition of Nickel-Based Layered Cathode Materials for Li-Ion Batteries. *J. Power Sources* **2006**, *163*, 219−222.
(9) Belharouak, I.; Vissers, D.; Amine, K. Thermal Stability of the $Li(Ni_{0.8}Co_{0.15}Al_{0.05})O_2$ Cathode in the Presence of Cell Components. *J. Electrochem. Soc.* **2006**, *153*, A2030−A2035.
(10) Belharouak, I.; Lu, W.; Vissers, D.; Amine, K. Safety Characteristics of $Li(Ni_{0.8}Co_{0.15}Al_{0.05})O_2$ and $Li(Ni_{1/3}Co_{1/3}Mn_{1/3})O_2$. *Electrochem. Commun.* **2006**, *8*, 329−335.
(11) Guilmard, M.; Croguennec, L.; Denux, D.; Delmas, C. Thermal Stability of Lithium Nickel Oxide Derivatives. Part I: $Li_xNi_{1.02}O_2$ and $Li_xNi_{0.89}Al_{0.16}O_2$ (x= 0.50 and 0.30). *Chem. Mater.* **2003**, *15*, 4476−4483.
(12) Belharouak, I.; Lu, W.; Liu, J.; Vissers, D.; Amine, K. Thermal Behavior of Delithiated $Li(Ni_{0.8}Co_{0.15}Al_{0.05})O_2$ and $Li_{1.1}(Ni_{1/3}Co_{1/3}Mn_{1/3})_{0.9}O_2$ Powders. *J. Power Sources* **2007**, *174*, 905−909.
(13) Venkatraman, S.; Shin, Y.; Manthiram, A. Phase Relationships and Structural and Chemical Stabilities of Charged $Li_{1-x}CoO_{2-\delta}$and $Li_{1-x}Ni_{0.85}Co_{0.15}O_{2-\delta}$Cathodes. *Electrochem. Solid-State Lett.* **2003**, *6*, A9−A12.
(14) Wu, L.; Nam, K.-W.; Wang, X.; Zhou, Y.; Zheng, J.-C.; Yang, X.-Q.; Zhu, Y. Structural Origin of Overcharge-Induced Thermal Instability of Ni-Containing Layered-Cathodes for High-Energy-Density Lithium Batteries. *Chem. Mater.* **2011**, *23*, 3953−3960.
(15) Hwang, S.; Chang, W.; Kim, S. M.; Su, D.; Kim, D. H.; Lee, J. Y.; Chung, K. Y.; Stach, E. A. Investigation of Changes in the Surface Structure of $Li_xNi_{0.8}Co_{0.15}Al_{0.05}O_2$ Cathode Materials Induced by the Initial Charge. *Chem. Mater.* **2014**, *26*, 1084−1092.
(16) Stach, E. A. Real-Time Observations with Electron Microscopy. *Mater. Today* **2008**, *11*, 50−58.
(17) Keast, V. J.; Scott, A. J.; Brydson, R.; Williams, D. B.; Bruley, J. Electron Energy-Loss Near-Edge Structure−a Tool for the Investigation of Electronic Structure on the Nanometre Scale. *J. Microsc.* **2001**, *203*, 135−175.
(18) Abraham, D. P.; Twesten, R. D.; Balasubramanian, M.; Kropf, J.; Fischer, D.; McBreen, J.; Petrov, I.; Amine, K. Microscopy and Spectroscopy of Lithium Nickel Oxide-Based Particles Used in High Power Lithium-Ion Cells. *J. Electrochem. Soc.* **2003**, *150*, A1450−A1456.
(19) Koyama, Y.; Mizoguchi, T.; Ikeno, H.; Tanaka, I. Electronic Structure of Lithium Nickel Oxides by Electron Energy Loss Spectroscopy. *J. Phys. Chem. B* **2005**, *109*, 10749−10755.
(20) Yoon, W.-S.; Chung, K. Y.; McBreen, J.; Fischer, D. A.; Yang, X.-Q. Electronic Structural Changes of the Electrochemically Li-Ion Deintercalated $LiNi_{0.8}Co_{0.15}Al_{0.05}O_2$ Cathode Material Investigated by X-ray Absorption Spectroscopy. *J. Power Sources* **2007**, *174*, 1015−1020.
(21) Arai, H.; Okada, S.; Sakurai, Y.; Yamaki, J.-I. Thermal Behavior of $Li_{1-y}NiO_2$ and the Decomposition Mechanism. *Solid State Ionics* **1998**, *109*, 295−302.
(22) Ohzuku, T.; Ueda, A.; Nagayama, M. Electrochemistry and Structural Chemistry of $LiNiO_2$ ($R\bar{3}m$) for 4 V Secondary Lithium Cells. *J. Electrochem. Soc.* **1993**, *140*, 1862−1870.
(23) Ostyn, K. M.; Carter, C. B. On the Reduction of Nickel Oxide. *Surf. Sci.* **1982**, *121*, 360−374.
(24) Kurata, H.; Lefevre, E.; Colliex, C.; Brydson, R. Electron-Energy-Loss Near-Edge Structures in the Oxygen K-edge Spectra of Transition-Metal Oxides. *Phys. Rev. B* **1993**, *47*, 13763−13768.